On the Impact of the Dead-Band of Power System Stabilizers and Frequency Regulation on Power System Stability

Muyang Liu, *IEEE Student Member*, Federico Bizzarri, *IEEE Senior Member*, Angelo Brambilla, *IEEE Member*, and Federico Milano, *IEEE Fellow*

Abstract— This letter studies the impact of the dead-band in the input signal of Power System Stabilizers (PSSs) on the transient response of power systems. The letter provides a taxonomy of the dynamic behavior of the system in various scenarios: no PSS, PSS without dead-band, and PSS with dead-band. For the latter, the dead-band stability margin and the interaction of the PSS with the system loading level as well as primary and secondary frequency regulators are discussed. The oscillatory behavior of the system is rigorously studied through the monodromy matrix and limit cycles are characterized by means of Floquet multipliers. The IEEE 14-bus system serves to illustrate the aforementioned scenarios.

Index Terms— Power System Stabilizer (PSS), dead-band, frequency control, limit cycle, monodromy matrix, Floquet multipliers.

I. INTRODUCTION

Dead bands are often utilized in power systems to reduce the operation and maintenance costs of mechanical devices such as Turbine Governors (TGs). The importance of dead-bands on primary frequency regulation and system stability is an ever-green topic that has been studied in the last six decades [1], [2]. Other uses of the dead-band are in PSSs, in particular, those for wide-area systems [3].

While the impact of communication delays on the stability of PSSs has been widely studied in recent years [4], [5], no study has focused so far on the impact of modelling a dead-band in the input signal of PSSs. This letter aims at filling this gap.

II. THEORETICAL BACKGROUND

The power system is modelled as a set of hybrid nonlinear Differential Algebraic Equations (DAEs) [6]:

$$\begin{bmatrix} \dot{\boldsymbol{x}} \\ \boldsymbol{0} \\ \dot{\boldsymbol{u}} \end{bmatrix} = \begin{bmatrix} \boldsymbol{f}(\boldsymbol{x}, \boldsymbol{y}, \boldsymbol{u}) \\ \boldsymbol{g}(\boldsymbol{x}, \boldsymbol{y}, \boldsymbol{u}) \\ \boldsymbol{0} \end{bmatrix} \ , \tag{1}$$

where $\boldsymbol{f} : \mathbb{R}^{n_x+n_y+n_u} \mapsto \mathbb{R}^{n_x}$ are differential equations; $\boldsymbol{g} : \mathbb{R}^{n_x+n_y+n_u} \mapsto \mathbb{R}^{n_y}$ are the algebraic equations; $\boldsymbol{x} \in \mathbb{R}^{n_x}$, $\boldsymbol{y} \in \mathbb{R}^{n_y}$ and $\boldsymbol{u} \in \mathbb{R}^{n_u}$ are state, algebraic and discrete variables, respectively. Variables $\boldsymbol{u}$ are in steady state except for a finite set of instants at which they *jump*, thus making $\boldsymbol{f}$ and $\boldsymbol{g}$ piecewise-smooth functions. These discrete events can be monitored by a proper set of n_h (n_x+n_y)-dimensional manifolds $\boldsymbol{h}(\boldsymbol{x}, \boldsymbol{y}) = 0$, where $\boldsymbol{h}(\boldsymbol{x}, \boldsymbol{y}) : \mathbb{R}^{n_x+n_y} \mapsto \mathbb{R}^{n_h}$. When a trajectory in the state space hits one of the n_h manifolds [say $h_j(\boldsymbol{x}, \boldsymbol{y}) = 0$] at $t = t_1$, $\boldsymbol{u}_1^-$ (i.e., $\boldsymbol{u}(t_1)$ immediately before the event) is instantaneously mapped in $\boldsymbol{u}_1^+ = \boldsymbol{b}_j(\boldsymbol{x}(t_1), \boldsymbol{y}(t_1), \boldsymbol{u}_1^-)$, where $\boldsymbol{b}_j : \mathbb{R}^{n_x+n_y+n_u} \mapsto \mathbb{R}^{n_u}$ (for $j = 1, ..., n_h$) are reset functions. To model the aforementioned manifolds, one can usually adopt *if-then* rules as in hybrid automata [6], [7]. In this letter, $\boldsymbol{u}$ is used to model the dead-bands.

Whenever (1) admits a T-periodic solution, say $\boldsymbol{\gamma}_T$, e.g., a limit cycle, its stability can be studied through the Floquet multipliers, i.e., the eigenvalues of its monodromy matrix. To provide the reader with some basic concepts on this topic, we focus on sets of hybrid nonlinear Ordinary Differential Equations (ODEs) thus neglecting $\boldsymbol{y}$ and $\boldsymbol{g}(\cdot, \cdot, \cdot)$. The interested reader can refer to [8] for a deeper overview concerning DAEs.

Let us first introduce the fundamental solution matrix for smooth ODEs, i.e., let us assume that $\boldsymbol{u}$ never jumps. In this case (1) reduces to $\dot{\boldsymbol{x}} = \boldsymbol{f}(\boldsymbol{x})$ with initial condition $\boldsymbol{x}(t_0) = \boldsymbol{x}_0$, and its $\boldsymbol{\Phi}(t, t_0)$ fundamental solution matrix is the solution of the *variational equation*:

$$\dot{\boldsymbol{\Phi}}(t, t_0) = \mathbf{J_f} \, \boldsymbol{\Phi}(t, t_0) \ , \tag{2}$$

with the initial condition $\boldsymbol{\Phi}(t_0, t_0) = \mathbf{1}_{n_x}$, where $\mathbf{J_f}$ is the Jacobian matrix of $\boldsymbol{f}$ and $\mathbf{1}_{n_x}$ is the $n_x \times n_x$ identity matrix. $\boldsymbol{\Phi}(t, t_0)$ provides the sensitivity of the solution of $\dot{\boldsymbol{x}} = \boldsymbol{f}(\boldsymbol{x})$ w.r.t. $\boldsymbol{x}_0$. If $\boldsymbol{x}(t_0) \in \boldsymbol{\gamma}_T$, then $\boldsymbol{x}(t_0) = \boldsymbol{x}(t_0 + T)$ and $\boldsymbol{\Phi}(T + t_0, t_0) \equiv \boldsymbol{\Psi}$ is called *monodromy matrix* and its eigenvalues are the μ_k ($k = 1, ..., n_x$) *Floquet multipliers* associated to $\boldsymbol{\gamma}_T$. If the condition $|\mu_k| \leq 1 \; \forall k$ holds, then $\boldsymbol{\gamma}_T$ is a stable limit cycle [9].

The computation of the fundamental solution matrix can be achieved using forward sensitivity analysis [10]. The variational equation (2) can be numerically integrated in parallel with the ODE originating it. Nevertheless, this approach is time-consuming as far as the dimension of the system gets big. To overcome this issue, the solution of the variational equation can be conveniently obtained as a by-product of the integration of the original ODE [11].[1]

If variables $\boldsymbol{u}$ are considered, thus leading to hybrid ODEs, the computation of $\boldsymbol{\Psi}$ is less straightforward since $\mathbf{J_f}$ is not defined at the points where $\boldsymbol{u}$ jumps and $\boldsymbol{f}$ is not continuous. Let us assume again that an event occurs for $t = t_1$. If the hybrid ODE admits a limit cycle $\boldsymbol{\gamma}_T$ with single switching point of $\boldsymbol{f}$ at $\boldsymbol{x}_1$, occurring at $t_1 \in (t_0, t_0 + T)$, then $\boldsymbol{\Psi}$ is computed as $\boldsymbol{\Phi}(T + t_0, t_1) \, \mathbf{S} \, \boldsymbol{\Phi}(t_1, t_0)$ where $\mathbf{S}$ is the *saltation matrix* operator, viz. a proper correction factor to be inserted whenever the trajectory hits one of the $\boldsymbol{h}(\boldsymbol{x}) = \boldsymbol{0}$ manifolds in the state space [12]. The trajectory hits $h_j(\boldsymbol{x}) = 0$ at $t = t_1$ and the saltation matrix is computed as:

$$\mathbf{S} = \mathbf{J_{b_j}} + \frac{\left(\begin{bmatrix} \boldsymbol{f}(\boldsymbol{x}_1, \boldsymbol{u}_1^+) \\ \boldsymbol{0} \end{bmatrix} - \mathbf{J_{b_j}} \begin{bmatrix} \boldsymbol{f}(\boldsymbol{x}_1, \boldsymbol{u}_1^-) \\ \boldsymbol{0} \end{bmatrix} \right) \begin{bmatrix} \nabla h_j \\ \boldsymbol{0} \end{bmatrix}^{\mathrm{T}}}{\nabla h_j{}^{\mathrm{T}} \boldsymbol{f}(\boldsymbol{x}_1, \boldsymbol{u}_1^-)} \ , \tag{3}$$

where $\mathbf{J_{b_j}}$ is the Jacobian of $\boldsymbol{b}_j$ computed at $(\boldsymbol{x}_1, \boldsymbol{u}_1^-)$, ∇h_j is the gradient of $h_j(\boldsymbol{x}) = 0$ computed at $\boldsymbol{x}_1$ and T is the transposition operator.

III. CASE STUDY

The analysis is based on the well-known IEEE 14-bus system, whose base-case model and data can be found in [6]. The system includes five synchronous machines with 6th order models. Each

---

[1] The PAN circuit simulator utlized for the simulations discussed in Section III implements this approach.

machine includes a IEEE DC1 Automatic Voltage Regulator (AVR). A PSS is installed for the generator connected at Bus 1. Generators 1 and 2 also include a steam turbine and a TG with servo motor and droop control and dead-band, $db_{TG} = 0.001$ pu(Hz), on the input frequency signal. Time-domain simulations are performed with Dome [13], whereas the shooting analysis was carried out and Floquet multipliers were calculated with the PAN simulator [14], [15].

The control scheme of the PSS with dead-band is shown in Fig. 1. A non-step dead-band model is considered:

$$\hat{\omega} = \begin{cases} 0, & -db_{PSS} \leq \omega \leq db_{PSS} \\ \omega - db_{PSS}, & \omega > db_{PSS} \\ \omega + db_{PSS}, & \omega < -db_{PSS} , \end{cases} \quad (4)$$

where ω is the rotor speed of the synchronous machine to which the PSS is connected.
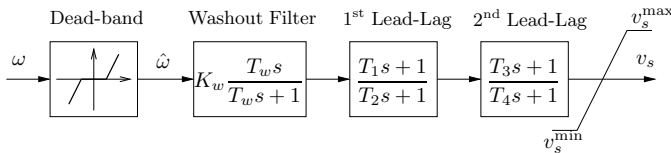
Fig. 1.   Power system stabilizer control diagram.

Increasing the loading level by 21% with respect to the base case makes the IEEE 14-bus system unstable without the PSS and the outage of line 2-5 gives birth to undamped oscillations at 2.93 Hz, as shown in Fig. 2. The PSS without dead-band ($db_{PSS} = 0$) is able to fully damp the electromechanical oscillations. One can think of the case with no PSS as a situation where the PSS has a very large dead-band ($db_{PSS} \to \infty$), such that the frequency error signal is always smaller than the dead-band itself and the PSS remains inactive.
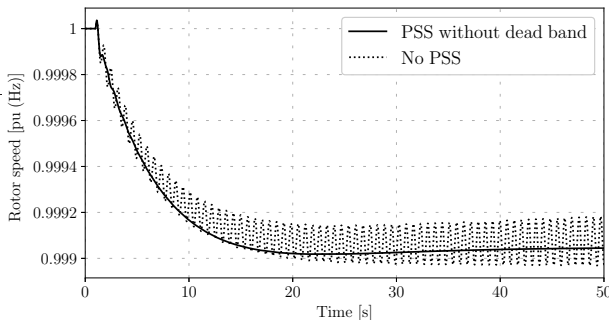
Fig. 2.   Line 2-5 outage for IEEE 14 bus system – Trajectories of the rotor speed of the synchronous generator at bus 1 for different scenarios: no PSS and PSS without dead-band connected to Generator 1.

Intuitively, since the system is stable for $db_{PSS} = 0$ and unstable for $db_{PSS} \to \infty$, there has to be a critical value $db_c > 0$ that defines the boundary between the stable and unstable conditions. Through time-domain simulations, we find $db_c \approx 0.000955$ pu(Hz) in this scenario. Figure 3 shows the dynamic behavior of the IEEE 14-bus system with PSS dead-bands slightly above and below the critical value db_c: following the line outage, the system with $db = 0.00095$ pu(Hz) is cheracterized by damped oscillations, while $db = 0.001$ pu(Hz) leads to a limit cycle with frequency 1.44 Hz.

Finally, Fig. 4 shows the impact of different values of the dead-band of the TG and the effect of the Automatic Generation Control (AGC) for the case of a PSS with $db = 0.00095$ pu(Hz).
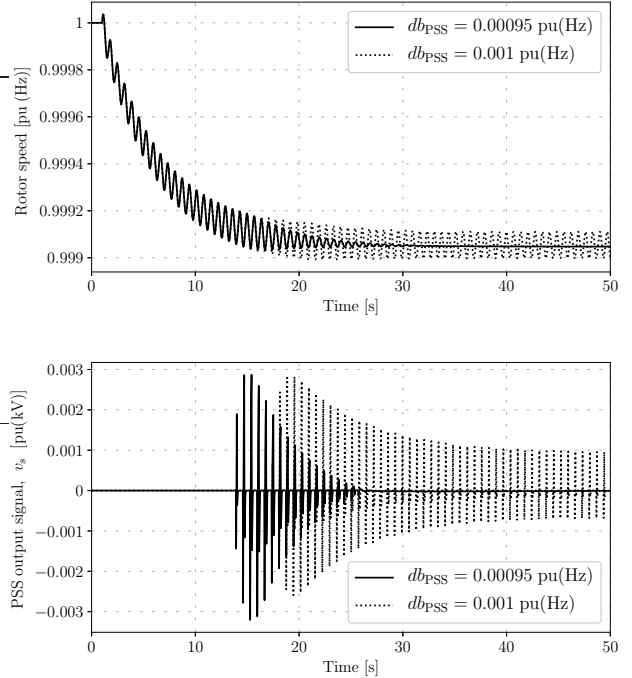
Fig. 3.   Line 2-5 outage for IEEE 14 bus system – Trajectories of the rotor speed of the synchronous generator at bus 1 with a PSS and PSS output signal for different values of db_{PSS}.
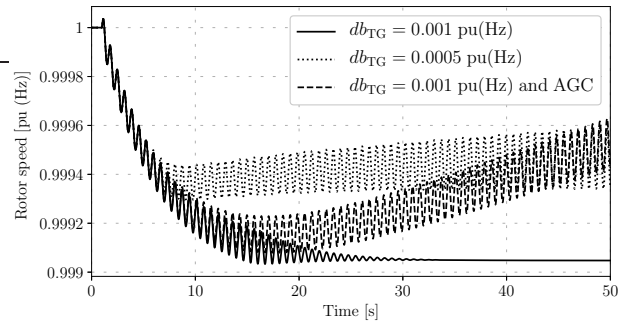
Fig. 4.   Line 2-5 outage for IEEE 14 bus system – Trajectories of the rotor speed of the synchronous generator at bus 1 with PSS with $db_{PSS} = 0.00095$ pu(Hz) for different scenarios: TGs with $db_{TG} = 0.001$ pu(Hz), TGs with dead-band 0.0005 pu(Hz); and TGs with $db_{TG} = 0.001$ pu(Hz) and AGC.

A. Stability Analysis of the Limit Cycles

We did time-domain shooting analyses to check if the oscillatory transient behaviors presented in this case study go toward a limit cycle. The shooting method heavily grounds on the computation of the fundamental solution matrix as outlined in the previous section and detailed in [8]. This analysis provides both the limit cycle and its $\boldsymbol{\Psi}$ monodromy matrix and, thus, also the Floquet multipliers.

As far as the "No PSS" scenario in Fig. 2 is concerned, by neglecting the Floquet multipliers $\mu_1 = \mu_2 = 1.00$, which are always present,[2] the Floquet multiplier with largest modulus is $\mu_3 = 0.986$. In this case no saltation matrices are needed since no dead-bands are present. Concerning the $db_{PSS} = 0.001$ pu(Hz) scenario, $\mu_3 = 0.989$

[2]The presence of $\mu_1 = 1$ is a direct consequence of the fact that (1) models an *autonomous* system, viz. the time variable t does not explicitly appear in it. The presence of $\mu_2 = 1$ is more involved. It is the counterpart of the always null eigenvalue of the Jacobian matrix of the power system linearized at any power flow solution [14].

and two saltation matrices are inserted along the limit cycle. The saltation matrices are required because of the discontinuities of some Jacobian matrix elements introduced by the dead-band of the PSS, as shown in the lower pane of Fig. 3 and Fig. 5. As for the scenarios with $db_{\mathrm{TG}} = 0.0005$ pu(Hz) and with AGC, i.e., the dotted and dashed lines shown in Fig. 4, they are both characterized by $\mu_3 = 0.986$.

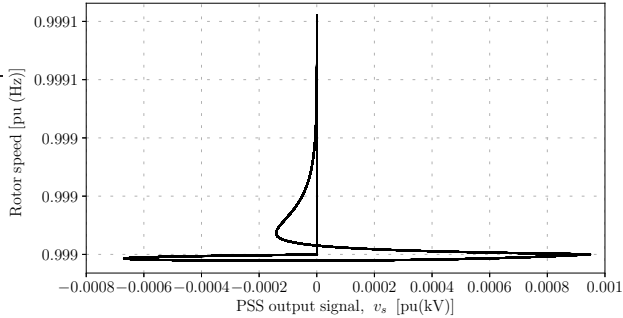Fig. 5. Limit cycle in the state space of the rotor speed of machine 1 and the PSS output signal with $db_{\mathrm{PSS}} = 0.001$ pu(Hz).

These results confirm that the steady-state oscillations are in fact stable limit cycles. The limit cycles of all oscillatory cases are due to the dynamic interaction of the AVR of the first synchronous generator with machine rotor flux dynamics. This leads to very similar Floquet multipliers in all these scenarios.

B. Taxonomy of the System Stability

Simulation results suggest the following taxonomy of the stability of the system after the line outage.

1) *System without PSS.* The system has no stable equilibrium point and the trajectories of the system after the contingency fall into a stable limit cycle.

2) *System with PSS without dead-band.* If properly tuned, the PSS makes the post-contingency equilibrium point stable and thus damps the trajectories of the variables of the system.

3) *System with PSS and "small" dead-band.* The dead-band makes the PSS insensitive at the beginning of the transient after the line outage. However, the power unbalance due to the increment of losses in the system and the non-perfect tracking behavior of the primary frequency control provided by TGs lead the frequency of the system to leave the dead-band of the PSS, which thus is able to damp the oscillations and to drive the system to a new stable equilibrium point.

4) System with PSS and "large" dead-band. The initial part of the transient is similar to the case with "small" dead-band. However, the trajectory of the rotor speed of generator 1 enters and leaves the dead-band region of the PSS. Inside the dead-band the trajectory is repelled by the unstable equilibrium that exists without PSS. Then the rotor speed moves away from the dead-band region. At this point, the PSS is enabled and the rotor speed is attracted by the newly formed stable equilibrium point. While moving along its trajectory the rotor speed returns inside the dead-band region. These events repeat periodically and cause the oscillatory behavior shown in Fig. 3.

In the above taxonomy, "small" and "large" are relative to the critical value of the dead-band, namely 0.000955 pu(Hz). Due to the nonlinearity of the system, there is no way to determine *a priori* whether a dead-band value will lead to a stable or an unstable equilibrium point for a given loading level and operating condition. However, there will always be a critical value that discriminates between stable and unstable conditions if the system, as in this case, is stable for $db = 0$ and unstable for $db = \infty$.

The effect of the dead-band on the stability of the system is deeply intertwined with the dynamics and parameters of the primary frequency regulation as well as the loading level of the system. As discussed above, it is the combination of the value of the dead-bands, the droop coefficient of the TGs of the synchronous generators and the power unbalance following the contingency to discriminate between a stable or unstable post-contingency equilibrium point and/or the birth of a stable limit cycle.

A small primary frequency control droop or a small db_{TG} can drive the system to instability even for small values of db_{PSS}. This fact also suggests that the effect of the AGC, whose objective is to reduce the frequency error to zero by varying the power set-point of the turbine of synchronous generators, is to destabilize the system, at least on the long term, regardless the value of the PSS dead-band. The effect of a smaller dead-band of the TGs as well as the effect of the AGC are shown in Fig. 4. These results indicate the counterintuitive conclusion that the design of the parameters of the PSS and, in particular, of its dead-band, has to be carefully coordinated with the design of primary and secondary frequency regulators. In future work, we will consider the impact of anti-dead-band controllers for PSSs such as the ones proposed in [1] to compensate the dead-band of the TGs of synchronous machines.

REFERENCES

[1] W. Tan, S. Chang, and R. Zhou, "Load frequency control of power systems with non-linearities," *IET Generation, Transmission Distribution*, vol. 11, no. 17, pp. 4307–4313, 2017.

[2] P. Bhui, N. Senroy, A. K. Singh, and B. C. Pal, "Estimation of inherent governor dead-band and regulation using unscented Kalman filter," *IEEE Trans. on Power Systems*, vol. 33, no. 4, pp. 3546–3558, July 2018.

[3] J. Zhang, C. Y. Chung, C. Lu, K. Men, and L. Tu, "A novel adaptive wide area pss based on output-only modal analysis," *IEEE Trans. on Power Systems*, vol. 30, no. 5, pp. 2633–2642, Sept. 2015.

[4] S. Wang, X. Meng, and T. Chen, "Wide-area control of power systems through delayed network communication," *IEEE Trans. on Control Systems Technology*, vol. 20, no. 2, pp. 495–503, Mar. 2012.

[5] M. Liu, I. Dassios, G. Tzounas, and F. Milano, "Stability analysis of power systems with inclusion of realistic-modeling wams delays," *IEEE Trans. on Power Systems*, vol. 34, no. 1, pp. 627–636, Jan. 2019.

[6] F. Milano, *Power System Modelling and Scripting*. London: Springer, 2010.

[7] I. A. Hiskens, "Power system modeling for inverse problems," *IEEE Trans. on Circuits and Systems I: Regular Papers*, vol. 51, no. 3, pp. 539–551, Mar. 2004.

[8] F. Bizzarri, A. Brambilla, and G. Storti Gajani, "Steady state computation and noise analysis of analog mixed signal circuits," *IEEE Trans. on Circuits and Systems I: Regular Papers*, vol. 59, no. 3, pp. 541 –554, Mar. 2012.

[9] M. Farkas, *Periodic motions*. New York, NY, USA: Springer-Verlag New York, Inc., 1994.

[10] T. Maly and L. R. Petzold, "Numerical methods and software for sensitivity analysis of differential-algebraic systems," *Applied Numerical Mathematics*, vol. 20, no. 1, pp. 57 – 79, 1996.

[11] T. Aprille and T. Trick, "A computer algorithm to determine the steady-state response of nonlinear oscillators," *IEEE Trans. on Circuit Theory*, vol. 19, no. 4, pp. 354 – 360, July 1972.

[12] M. Di Bernardo, C. Budd, A. Champneys, and P. Kowalczyk, *Piecewise-smooth Dynamical Systems, Theory and Applications*. London: Springer-Verlag, 2008.

[13] F. Milano, "A Python-based software tool for power system analysis," in *Procs. of the IEEE PES General Meeting*, Vancouver, BC, July 2013.

[14] F. Bizzarri, A. Brambilla, and F. Milano, "The probe-insertion technique for the detection of limit cycles in power systems," *IEEE Trans. on Circuits and Systems - I: Regular Papers*, vol. 63, no. 2, pp. 312–321, Feb. 2016.

[15] F. Bizzarri, A. Brambilla, G. S. Gajani, and S. Banerjee, "Simulation of real world circuits: Extending conventional analysis methods to circuits described by heterogeneous languages," *IEEE Circuits and Systems Magazine*, vol. 14, no. 4, pp. 51–70, Q4 2014.